Computations of the first eigenpairs for the Schrödinger operator with magnetic field

V. Bonnaillie-Noël, M. Dauge, D. Martin and G. Vial

Abstract

This paper is devoted to computations of eigenvalues and eigenvectors for the Schrödinger operator with constant magnetic field in a domain with corners, as the semi-classical parameter h tends to 0. The eigenvectors corresponding to the smallest eigenvalues concentrate in the corners: They have a two-scale structure, consisting of a corner layer at scale $\sqrt{h}$ and an oscillatory term at scale h. The high frequency oscillations make the numerical computations particularly delicate. We propose a high order finite element method to overcome this difficulty. Relying on such a discretization, we illustrate theoretical results on plane sectors, squares, and other straight or curved polygons. We conclude by discussing convergence issues.

1 Introduction

Superconductivity theory, modeled by Ginzburg and Landau, motivates investigations of the Schrödinger operator with magnetic field and Neumann boundary conditions in two-dimensional domains. The Schrödinger operator $-(h\nabla - i\mathcal{A})^2$ derives from a linearization of the Ginzburg-Landau functional and the behavior of its eigenvalues and eigenvectors as $h \to 0$ gives information about the onset of superconductivity in the material, see [6, 7, 13, 14, 20, 29] for the general framework and [2, 15, 16, 17, 18, 19, 24, 26, 28] for more closely related questions concerning the Schrödinger operator.

We give the mathematical framework we will work within: let Ω denote a bounded polygonal domain in $\mathbb{R}^2$ and $\mathcal{A}$ the magnetic potential $\frac{1}{2}(-x_2, x_1)$ defined on $\mathbb{R}^2$. We investigate the behavior of the eigenpairs of the Neumann realization P_h on Ω for the Schrödinger operator $-(h\nabla - i\mathcal{A})^2$ as $h \to 0$. The variational space associated with P_h is $H^1(\Omega)$ and its domain is the subspace of functions u such that $P_h u \in L^2(\Omega)$ and $\nu \cdot (h\nabla - i\mathcal{A})u = 0$ on $\partial\Omega$, with ν denoting the unit normal to $\partial\Omega$.

Let us first mention that the Schrödinger operator P_h is gauge invariant in the sense of the following proposition:

Proposition 1.1. *Let $\phi \in H^2(\Omega)$, then u is an eigenvector associated with the eigenvalue μ for the operator $-(h\nabla - i\mathcal{A})^2$ if and only if $u_\phi := \mathrm{e}^{i\phi/h}u$ is an eigenvector associated with the eigenvalue μ for the operator $-(\nabla - i(\mathcal{A} + \nabla\phi))^2$.*

In particular, the eigenvalues of the Schrödinger operator are the same for any potential $\tilde{\mathcal{A}}$ such that $\operatorname{curl}\tilde{\mathcal{A}} = \operatorname{curl}\mathcal{A}$. This allows the use of adapted gauges according to the domain.

In [10], a complete asymptotic expansion of low-lying eigenstates is exhibited for curvilinear polygonal domains and refined results are proved in the case when the domain has straight sides and the magnetic field is constant. The eigenmodes have a two-scale structure, in the form of the product of a corner layer at scale $\sqrt{h}$ with an oscillatory term at scale h. The latter makes the numerical approximation delicate. *A posteriori* error estimates are used in [3, 9] to determine localized mesh refinement in a low degree finite element method. We investigate here a finite element method using high degree polynomials, as described in Section 2.

It is proved in [10] that the study of the Schrödinger operator P_h in a domain with corners of openings $\alpha_1, \ldots, \alpha_J$, relies on those of the Schrödinger operator $Q^\alpha := -(\nabla - i\mathcal{A})^2$ on an infinite sector of opening α, for $\alpha = \alpha_1, \ldots, \alpha_J$. Section 3 is devoted to this operator: We show computations which make theoretical results more complete.

The next sections deal with the asymptotic behavior of the eigenstates of P_h as h goes to 0: We give numerical solutions which illustrate the clustering of eigenvalues, depending on the symmetries of the domain. Several particular polygonal domains are investigated, highlighting different points of the theory: Tunneling effect for the square, concentration in the lowest corners for the trapezoid, the rhombus or the L-shaped domain. We end with a curvilinear polygon for which the asymptotics is appreciably different.

We conclude the paper in Section 7 by numerical error curves for the specific case of a standard square of length 2, and $h = 0.02$. We compare the performances of "p-extensions" (increasing the polynomial degree on a fixed mesh), and of "h-extensions" (refining the mesh with a fixed degree). According to the magnitude of h, a locking phenomenon is present, stronger and stronger as $h \to 0$. A disturbing feature of this locking is the preasymptotic convergence to interior modes, corresponding to the lowest Landau level, significantly larger than the correct eigenvalues. Our conclusion is the necessity for using "p-extensions" if we wish to capture fine effects like the tunneling effect in symmetric domains.

2 General results on eigenvalue approximation

In the sequel, we will show numerical results of spectral approximations for the Schrödinger operator in various domains. We wish first to recall some facts on the numerical computation of eigenvalues and eigenvectors by a finite element Galerkin method, which serve as a basis to justify the relevance of our results.

Let us fix some notation:

- $\mu_{h,n}$ is the n-th eigenvalue of the operator P_h,
- $u_{h,n}$ is a normalized associated eigenfunction in $\mathcal{V} = H^1(\Omega)$,
- $(\mathcal{T}^\ell)_{\ell>0}$ is a family of quadrilateral meshes, where ℓ is the maximum size of the elements (we changed the traditional h into ℓ since the letter h already stands for the

small semi-classical parameter),

- $\mathbb{Q}_p$ is the standard space of polynomials of partial degree p in the reference square element,
- $\mathcal{V}^{\ell,p}$ is the conforming discrete variational space associated with the $\mathbb{Q}_p$-reference square element on the mesh $\mathcal{T}_\ell$,
- $(\mu_{h,n}^{\ell,p}, u_{h,n}^{\ell,p})$ is the n-th discrete eigenpair of P_h in $\mathcal{V}^{\ell,p}$:

$$\int_\Omega (h\nabla - i\mathcal{A})u_{h,n}^{\ell,p} \cdot \overline{(h\nabla - i\mathcal{A})v}\, dx = \mu_{h,n}^{\ell,p} \int_\Omega u_{h,n}^{\ell,p}\, \overline{v}\, dx, \quad \forall v \in \mathcal{V}^{\ell,p}.$$

For the first eigenpair ($n = 1$) or, more generally, if $\mu_{h,n} \neq \mu_{h,n-1}$, it is known from [4, 5, 11] that the following Céa-like estimate holds

$$|\mu_{h,n} - \mu_{h,n}^{\ell,p}| \leq L_{h,n}^{\ell,p} \sup_{u \in M_{h,n}} \inf_{\chi \in \mathcal{V}^{\ell,q}} \|u - \chi\|_{\mathcal{V}}^2, \tag{1}$$

where $M_{h,n}$ is the set of normalized eigenvectors[1] associated with $\mu_{h,n}$ and $L_{h,n}^{\ell,p}$ a positive constant which, for each fixed $h > 0$ and $n \in \mathbb{N}$, is bounded as $\ell \to 0$ or $p \to \infty$. Moreover the corresponding estimate for eigenvectors reads: There exists an eigenvector $\tilde{u}_{h,n}$ associated with $\mu_{h,n}$ satisfying

$$\|\tilde{u}_{h,n} - u_{h,n}^{\ell,p}\|_{\mathcal{V}} \leq L_{h,n}^{\ell,p} \sup_{u \in M_{h,n}} \inf_{\chi \in \mathcal{V}^{\ell,q}} \|u - \chi\|_{\mathcal{V}}. \tag{2}$$

Thus discretization errors on the eigenpairs are essentially bounded by the best approximation errors on the eigenvectors of P_h. We have to keep in mind that the latter closely depends on the semi-classical parameter h.

In the following, we will interpret the Galerkin approximations obtained for the eigenpairs, with respect to the asymptotic results of [10]. We emphasize the fact that, since by construction $\mathcal{V}^{\ell,p} \subset \mathcal{V}$, the computed eigenvalues will always be *greater* than the exact eigenvalue of same rank.

All the results displayed in this paper have been obtained with the Finite Elements Library Mélina, see [27]. Computations are mostly done with pretty coarse meshes (consisting of less than 100 quadrilaterals), but with high polynomial degree (10 in general, referred to as $\mathbb{Q}_{10}$-approximation). We justify our choice of a "p-extension" (where the degree p of polynomials is increased), rather than a "h-extension" (where the size ℓ of the elements is decreased), by the fact that – for the same number of degrees of freedom – a p-extension captures oscillations more accurately than a h-extension, see [1, 22, 23] for related questions concerning the Helmholtz equation and dispersion relations at high wave number. This point is discussed in more detail in Section 7.

3 Model operators in infinite sectors

This section is devoted to the study of the Schrödinger operator $-(\nabla - i\mathcal{A})^2$ in an infinite sector: The analysis of the operator P_h in a bounded domain with corners relies on this

[1] If $\mu_{h,n} = \mu_{h,n-1}$, the set $M_{h,n}$ has to be modified accordingly.

model situation. We first recall some theoretical results from [8] concerning the spectrum of the operator and, next, we show some numerical experiments which illustrate some of these results or give hints on how to extend them.

3.1 Theoretical results on sectors

We denote by $\mathsf{X} = (\mathsf{X}_1, \mathsf{X}_2)$ the Cartesian coordinates in $\mathbb{R}^2$, and by $R = |\mathsf{X}|$ and θ the polar coordinates. Let G^α be the sector in $\mathbb{R}^2$ with opening α:

$$G^\alpha = \{\mathsf{X} \in \mathbb{R}^2, \quad \theta \in (0, \alpha)\},$$

and Q^α be the Neumann realization of the Schrödinger operator $-(\nabla - i\mathcal{A})^2$ on the sector G^α. With the potential $\mathcal{A}(\mathsf{X}) = \frac{1}{2}(-\mathsf{X}_2, \mathsf{X}_1)$, the operator Q^α takes the form

$$Q^\alpha = -\Delta + i(\mathsf{X}_1 \partial_{\mathsf{X}_2} - \mathsf{X}_2 \partial_{\mathsf{X}_1}) + \frac{1}{4}|\mathsf{X}|^2.$$

The operator Q^α is associated with the following variational space

$$\mathcal{V}^\alpha = \big\{\Psi \in L^2(G^\alpha), \ \ (\nabla - i\mathcal{A})\Psi \in L^2(G^\alpha)\big\}, \ \ ||\Psi||^2_{\mathcal{V}^\alpha} = ||\Psi||^2_{L^2} + ||(\nabla - i\mathcal{A})\Psi||^2_{L^2}.$$

We denote by $\mu_k(\alpha)$ the k-th smallest element of the spectrum given by the max-min principle. We quote some results of [8] about the spectrum of Q^α.

Theorem 3.1.

(i) The infimum of the essential spectrum of Q^α is equal to $\Theta_0 := \mu_1(\pi)$.

(ii) For all $\alpha \in (0, \pi/2]$, $\mu_1(\alpha) < \Theta_0$ and, therefore, $\mu_1(\alpha)$ is an eigenvalue.

(iii) Let $\alpha \in (0, 2\pi)$ and $k \geq 1$. Let Ψ^α_k be an eigenfunction associated with $\mu_k(\alpha) < \Theta_0$ for the operator Q^α. Then Ψ^α_k satisfies the following exponential decay estimate:

$$\forall \varepsilon > 0, \ \exists C_{\varepsilon,\alpha} > 0, \quad \Big|\Big| \, \mathrm{e}^{\left(\sqrt{\Theta_0 - \mu_k(\alpha)} - \varepsilon\right)|\mathsf{X}|} \, \Psi^\alpha_k \Big|\Big|_{\mathcal{V}^\alpha} \leq C_{\varepsilon,\alpha}. \tag{3}$$

(iv) For all $\alpha \in (0, \pi]$,

$$\frac{\Theta_0}{\pi} \leq \frac{\mu_1(\alpha)}{\alpha} \leq \frac{1}{\sqrt{3}}, \tag{4}$$

and there holds

$$\frac{\mu_1(\alpha)}{\alpha} \to \frac{1}{\sqrt{3}} \quad as \quad \alpha \to 0. \tag{5}$$

Remark 3.2. Using the same technique as [8], one can establish asymptotics of the k-th eigenvalue as $\alpha \to 0$, similar to (5):

$$\frac{\mu_k(\alpha)}{\alpha} \to \frac{2k+1}{\sqrt{3}} \quad \text{as} \quad \alpha \to 0. \tag{6}$$

3.2 Numerical experiments on sectors

We present here some results of numerical computations of the low-lying eigenvalues, which illustrate the estimates (4), (5) and (6). Furthermore, it allows to investigate the monotonic behavior of $\mu_k(\alpha)$ with respect to the opening α.

The method we have used to compute approximations of the eigenvalues consists in a high order finite element method, using quadrilateral elements and tensor-product polynomials of degree 10. Let us explain the way we deal with the unboundedness of the domain: For a given α, we mesh a bounded cornered strip ω of opening α, see Figure 1, and, for any $h > 0$, we consider the scaled operator $Q^\alpha_{h,\omega}$ defined on ω as

$$Q^\alpha_{h,\omega} = -(h\nabla - i\mathcal{A})^2. \tag{7}$$

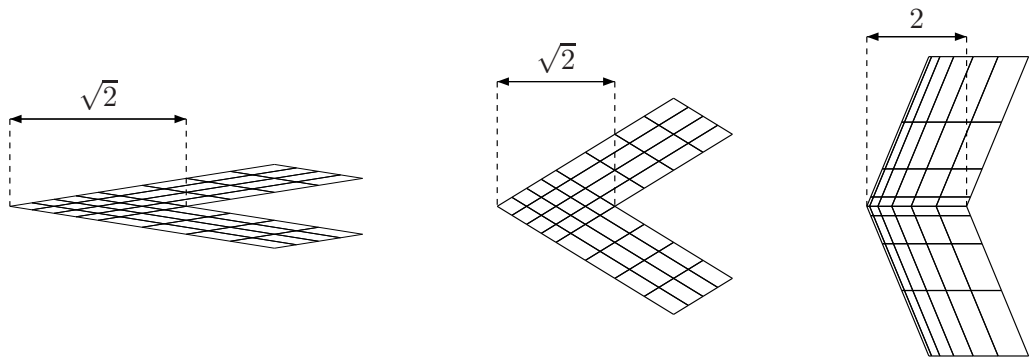

Figure 1: Meshes on cornered strips for $\alpha = 0.1\pi,\ 0.35\pi,\ 0.75\pi$.

By dilatation, the eigenvalues of the operator $Q^\alpha_{1,h^{-1}\omega}$ are the same as those of $Q^\alpha_{h,\omega}$ divided by h. Consequently, taking the decay of eigenvectors into account, we recover the eigenvalues of Q^α on the infinite sector G^α at the limit $h \to 0$. This formulation offers the advantage to be consistent with the analysis in the next sections for bounded domains.

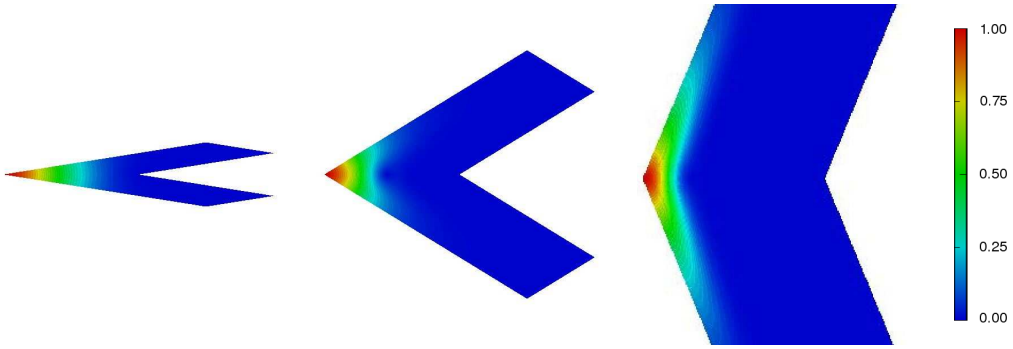

Figure 2: Moduli of the first eigenfunction for $\alpha = 0.1\pi,\ 0.35\pi,\ 0.75\pi$.

To ensure that the eigenvalues in the infinite sector are approximated from above, we impose Dirichlet boundary conditions on the edges of ω which differ from the boundary

of G^α (keeping natural Neumann conditions elsewhere). The choice of meshes such as in Figure 1 is justified by the localization of the eigenvectors given in Theorem 3.1. This exponential concentration is illustrated in Figure 2: We note that the behavior of the first eigenvector changes when the opening increases. Indeed, when the opening is small (e.g., $\alpha \leq \pi/10$ like in the left picture of Figure 2), the eigenvector appears to be essentially radial, in coherence with asymptotics as $\alpha \to 0$. When the opening increases, the modulus of the eigenvector spreads out along the boundary (see right picture of Figure 2). Consequently, we realize computations with two different meshes according to the opening (the mesh on the right of Figure 1 is refined near the edges where the eigenvector is expected to be mostly supported).

3.2.1 Asymptotics of $\mu_k(\alpha)$ as $\alpha \to 0$

In order to increase the accuracy of the approximation of the eigenvalues for small angles, we introduce a gauge transform which leads to the potential $\tilde{\mathcal{A}}(x) = (-x_2, 0)$. The resulting operator $\tilde{Q}^\alpha = -(\nabla - i\tilde{\mathcal{A}})^2$ has the same spectrum than Q^α, as explained in Proposition 1.1. The relevance of such a transform is linked to the amplitude of the potential: for small openings α, $\tilde{\mathcal{A}}$ is smaller than $\mathcal{A}$ in the considered domain. We expect a better approximation for $\tilde{Q}^\alpha$ than for Q^α since the associated eigenvectors are less oscillating.

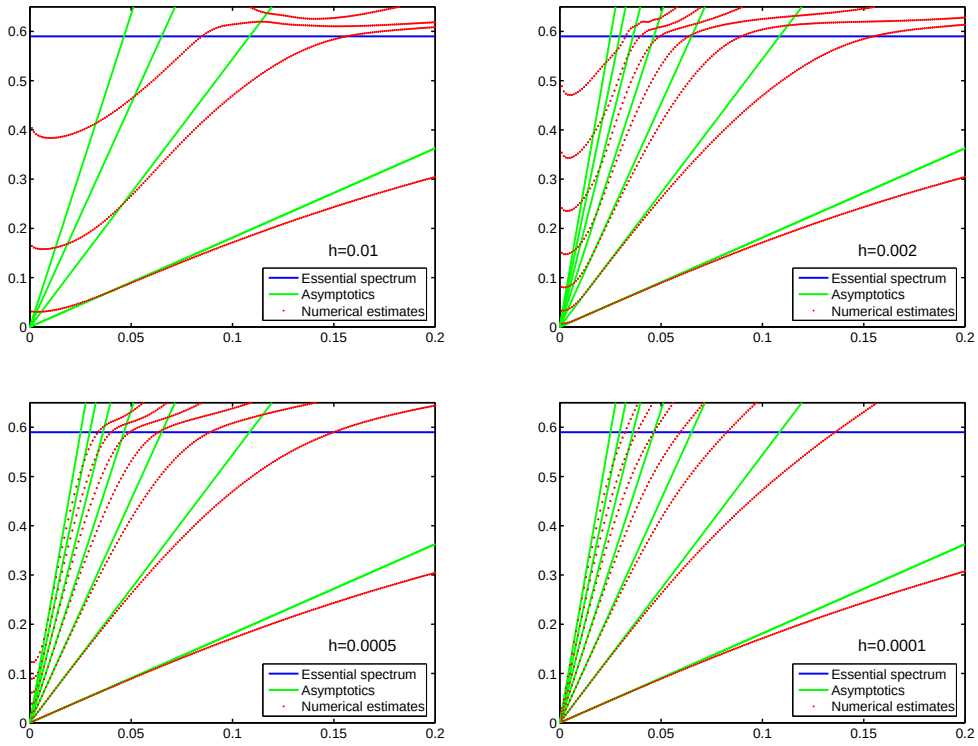

Figure 3: $\mu_k(\alpha)$ vs. $\frac{\alpha}{\pi}$, $k = 1, \ldots, 7$.

In Figure 3, we present numerical computations of $\mu_k(\alpha)$ for $k = 1, \cdots, 7$ and $\alpha \in$

$\{j\pi/1000, j = 1, \ldots, 200\}$ using $h = 0.01,\ 0.002,\ 0.0005,\ 0.0001$. We observe that we capture very precisely the asymptotics of $\mu_k(\alpha)$ given in (6) as soon as the parameter h is small. This is a consequence of the behavior of the eigenvectors recalled in Theorem 3.1: the eigenfunctions are localized near the corner and are exponentially small far from the corner. Consequently, the less h, the less information we lose, and the better the approximation of the eigenpairs.

The improvement of the approximation for small angles is clear in Figures 3, whereas the situation seems to be the reverse for larger values of α. Indeed, the eigenvalues being approximated from above, the results for $\alpha > \pi/10$ are deteriorating for small h. This phenomenon can be explained by the fact that we keep the same number of elements to capture higher oscillations: the mesh is too coarse to approximate accurately the eigenfunctions.

3.2.2 Monotonicity of $\alpha \mapsto \mu_1(\alpha)$

Let us now focus on the first eigenvalue. We have observed the asymptotic behavior (4) as $\alpha \to 0$ in Figure 3 for $\alpha \in (0, \pi/5)$. Figure 5 gives computations for $\alpha \in (0, \pi)$ with a discretization $\{j\pi/200, j = 1, \ldots, 200\}$. We have realized these computations with several values of h between 10^{-4} and 0.5 and three magnetic potentials $\mathcal{A}(x) = \frac{1}{2}(-x_2, x_1)$ (symmetric gauge), $\widetilde{\mathcal{A}}(x) = (-x_2, 0)$ and $\widehat{\mathcal{A}}(x) = (0, x_1)$ (Landau gauges). According to Proposition 1.1, the Schrödinger operator associated with these three potentials have the same spectrum and the eigenvectors can be easily deduced one from the other. We show in Figure 4 the effect of the gauge on the phase of the first eigenvector. The potential $\widetilde{\mathcal{A}}$ is better adapted for small openings ($\alpha < \pi/10$), the potential $\widehat{\mathcal{A}}$ is more convenient for large openings ($\alpha > 19\pi/20$) since the eigenvector is localized in the corner and also along the Neumann boundary. For the other openings, the potential $\mathcal{A}$ gives better results.

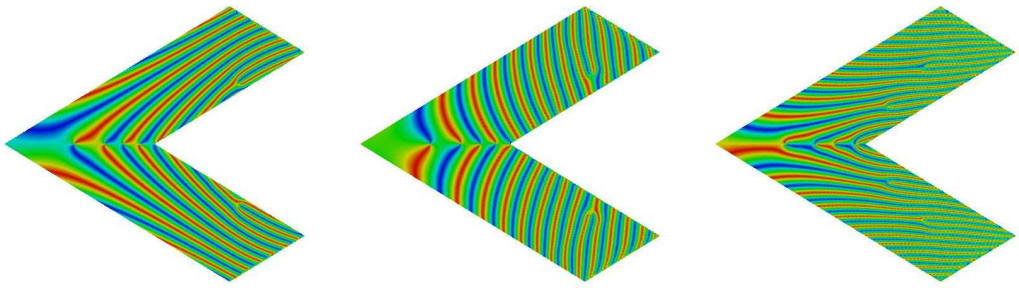

Figure 4: Phases of first eigenvector for gauges $\mathcal{A}$, $\widetilde{\mathcal{A}}$, $\widehat{\mathcal{A}}$.

The curve in Figure 5 plots the minimum value obtained from these configurations for any opening. We have also represented on the graph the bottom of the essential spectrum $\Theta_0 \simeq 0.5901$ and the lower and upper bounds given in (4). Since the numerical estimates for the bottom of the spectrum give an upper-bound of $\mu_1(\alpha)$, we are ensured that $\mu_1(\alpha) < \Theta_0$ for any $\alpha \in \{j\pi/200, j = 1, \ldots, 190\}$. We have gathered in Table 1 the value of $\mu_1(\alpha)$ obtained for $\alpha = j\pi/40$. The comparison between the numbers obtained with $\mathbb{Q}_9$ and $\mathbb{Q}_{10}$-

approximations provides an accuracy estimation for the computed eigenvalues. Numerical experiments for $\alpha \in [\pi, 6\pi/5]$ do not show eigenvalue less than Θ_0 with similar meshes as in Figure 1.

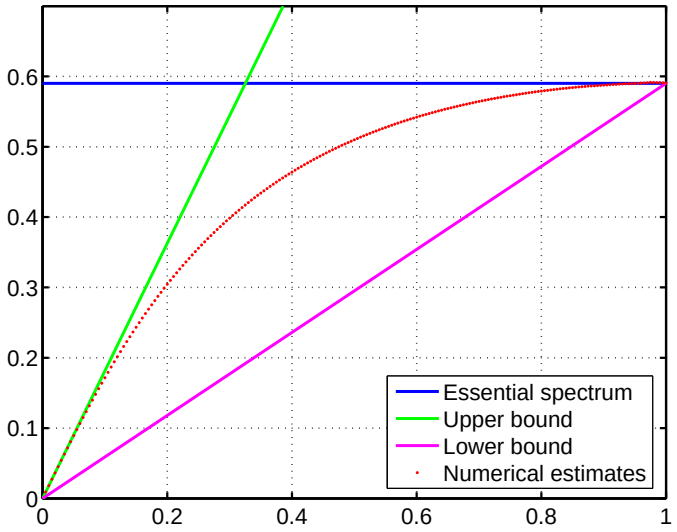

Figure 5: $\mu_1(\alpha)$ vs. $\frac{\alpha}{\pi}$ for $\alpha \in [0, \pi]$.

	$\mu_1\left(j\frac{\pi}{40}\right)$			$\mu_1\left(j\frac{\pi}{40}\right)$			$\mu_1\left(j\frac{\pi}{40}\right)$	
j	$\mathbb{Q}_9$	$\mathbb{Q}_{10}$	j	$\mathbb{Q}_9$	$\mathbb{Q}_{10}$	j	$\mathbb{Q}_9$	$\mathbb{Q}_{10}$
1	0.04516	0.04516	16	0.46400	0.46400	31	0.57623	0.57614
2	0.08930	0.08930	17	0.47704	0.47704	32	0.57924	0.57922
3	0.13160	0.13160	18	0.48898	0.48897	33	0.58193	0.58185
4	0.17153	0.17153	19	0.49990	0.49990	34	0.58430	0.58415
5	0.20883	0.20883	20	0.50991	0.50991	35	0.58632	0.58619
6	0.24339	0.24339	21	0.51907	0.51907	36	0.58819	0.58763
7	0.27524	0.27524	22	0.52745	0.52745	37	0.58997	0.58904
8	0.30447	0.30447	23	0.53512	0.53512	38	0.59030	0.59000
9	0.33123	0.33123	24	0.54213	0.54213	39	0.60130	0.59149
10	0.35570	0.35570	25	0.54853	0.54852	40	0.59087	0.59064
11	0.37806	0.37806	26	0.55435	0.55435			
12	0.39848	0.39848	27	0.55965	0.55964			
13	0.41713	0.41713	28	0.56445	0.56443			
14	0.43418	0.43418	29	0.56880	0.56876			
15	0.44976	0.44976	30	0.57272	0.57265			

Table 1: Numerical values for the bottom of the spectrum.

Remark 3.3. Considering the results in Figure 5, we conjecture that μ_1 is strictly increasing from $(0,\pi]$ onto $(0,\Theta_0]$, equal to Θ_0 on $[\pi,2\pi]$ and that $\mu_1'(\pi)=0$. Furthermore, from the results in Figure 3 it appears that there is only one eigenvalue $\mu_1(\alpha)$ below the essential spectrum for $\alpha\in(\pi/5,\pi)$.

4 Square

We consider here the Schrödinger operator $P_h=-(h\nabla-i\mathcal{A})^2$ with Neumann boundary conditions on the model square $\Omega_{\mathsf{sq}}=(-1,1)\times(-1,1)$, and the range 1 to 0.01 for the parameter h.

4.1 Theoretical results

We denote by $\mathsf{s}_1=(-1,-1)$, $\mathsf{s}_2=(1,-1)$, $\mathsf{s}_3=(1,1)$, $\mathsf{s}_4=(-1,1)$ the vertices of Ω_{sq}. The analysis of the eigenpairs of P_h on the square fits in the framework of more general polygonal domains, studied in [10]. We give here a specified version of the results, which takes into account the symmetry properties of the square.

Relying on Remark 3.3, we admit that there is only one eigenvalue $\mu_1(\pi/2)$ below Θ_0 for the operator $Q^{\pi/2}$ on the quarter plane and that $\mu_1(\pi/2)$ is simple. Corresponding to the 4 corners of the square, the first 4 eigenpairs of P_h derive from 4 *quasi-modes* generated by the eigenpair $\big(\mu_1(\pi/2),\Psi_1^{\pi/2}\big)$ on the quarter plane:

Notation 4.1. • Let $\mu_{h,n}$ be the n-th eigenvalue of P_h counted with multiplicity and $u_{h,n}$ be a normalized eigenfunction associated with $\mu_{h,n}$.
• We introduce the sum F_h of the first 4 eigenspaces of P_h:

$$F_h=\mathrm{span}\big\{u_{h,1},u_{h,2},u_{h,3},u_{h,4}\big\}.$$

• We define the corresponding space E_h of quasi-modes

$$E_h=\mathrm{span}\big\{\psi_{h,\mathsf{s}_1},\ \psi_{h,\mathsf{s}_2},\ \psi_{h,\mathsf{s}_3},\ \psi_{h,\mathsf{s}_4}\big\}$$

generated by the 4 functions ψ_{h,s_j} defined as follows: Let $j\in\{1,2,3,4\}$ and $\mathcal{R}_j$ be the rotation of opening $(j-1)\pi/2$. We first define the function $\breve{\psi}_{h,\mathsf{s}_j}$ by

$$\breve{\psi}_{h,\mathsf{s}_j}(x)\ =\ \frac{1}{\sqrt{h}}\exp\left(\frac{i}{2h}\,x\wedge\mathsf{s}_j\right)\ \Psi_1^{\pi/2}\left(\frac{\mathcal{R}_j(x-\mathsf{s}_j)}{\sqrt{h}}\right)\quad\text{on}\quad\mathcal{R}_j^{-1}G^{\pi/2}\tag{8}$$

and set

$$\psi_{h,\mathsf{s}_j}(x)=\chi_j(x)\,\breve{\psi}_{h,\mathsf{s}_j}(x)\quad\text{on}\quad\Omega_{\mathsf{sq}}.\tag{9}$$

Here χ_j is a radial smooth cut-off function with support in the ball $B(\mathsf{s}_j,2)$ and equal to 1 in $B(\mathsf{s}_j,2-\delta)$ for some positive δ.

The quasi-modes ψ_{h,s_j} allow to compare the eigenvalues of P_h with those of $Q^{\pi/2}$; the distance between the clusters E_h and F_h can be quantified as well. The results of [10] applied to the situation of a square give the estimates:

Proposition 4.2. *With Notation* 4.1*, for any* $\varepsilon > 0$*, there exist* $C_\varepsilon > 0$ *such that for* $n = 1, 2, 3, 4$*,*

$$\left|\mu_{h,n} - h\mu_1\left(\frac{\pi}{2}\right)\right| \leq C_\varepsilon \exp\left(-\frac{2\sqrt{\Theta_0 - \mu_1\left(\frac{\pi}{2}\right)} - \varepsilon}{\sqrt{h}}\right). \tag{10}$$

Furthermore, for any $\varepsilon \geq \delta$*:*

$$d(E_h, F_h) \leq C_\varepsilon \exp\left(-\frac{2\sqrt{\Theta_0 - \mu_1\left(\frac{\pi}{2}\right)} - \varepsilon}{\sqrt{h}}\right),$$

where d *is the distance defined by* $d(E_h, F_h) = ||\Pi_{E_h} - \Pi_{F_h}\Pi_{E_h}||_{\mathcal{H}}$*, with* Π_{E_h} *and* Π_{F_h} *the orthogonal projections onto* E_h *and* F_h *respectively.*

Consequently the eigenvectors associated with the smallest four eigenvalues of P_h are exponentially close to a linear combination of the four quasi-modes ψ_{h,s_j}, $j = 1, 2, 3, 4$. Numerical experiments show that these combinations are not trivial. Furthermore, this theorem also proves that the smallest four eigenvalues of P_h form a *cluster* exponentially close to $h\mu_1(\pi/2)$. Numerical experiments bring more information about the behavior of these eigenvalues, and display fine interactions. Moreover, although no theoretical results are available for eigenvalues of rank larger than 5 (except the fact that they cannot converge below $\Theta_0 \simeq 0.59$), we will see that they also organize into clusters of 4.

In the following, when representing eigenmodes, we show their moduli and, most often, their phases. The phase is computed according to the formula $\arcsin(\mathrm{Im}\,(z)/|z|)$.

4.2 Dependency on h of the first eigenfunction

Formula (8) exhibits a two-scale structure for the quasi-modes: a corner layer at scale $\sqrt{h}$ coming from the dilatation $\Psi_1^{\pi/2}(\cdot/\sqrt{h})$, and an oscillatory term at scale h due to $\mathrm{e}^{\frac{i}{2h}x\wedge\mathsf{s}}$. Relying on Proposition 4.2, the same holds for the functions in the eigenspace E_h. Consequently, especially because of harsh oscillations, there is a difficult issue of approximating correctly the eigenfunctions of P_h for small values of h.

We present as a conclusion of this paper in Section 7 a systematic investigation of errors when discretizing our problem on the square thanks to h-extensions with bilinear elements, or to p-extensions with coarse meshes of 1 to 64 elements. In this section, we choose each time an optimal combination mesh-degree to display eigenmodes.

To compute the first eigenfunction for $h = 0.1,\ 0.08,\ 0.06,\ 0.04,\ 0.02,\ 0.01$, we keep the polynomial approximation fixed to $\mathbb{Q}_{10}$ and a 8×8 mesh. Figure 6 gives the modulus of the first eigenfunction and Figure 7 its phase. As expected, we observe that the modulus is more and more concentrated in the corners and phase has sharper oscillations when h decreases.

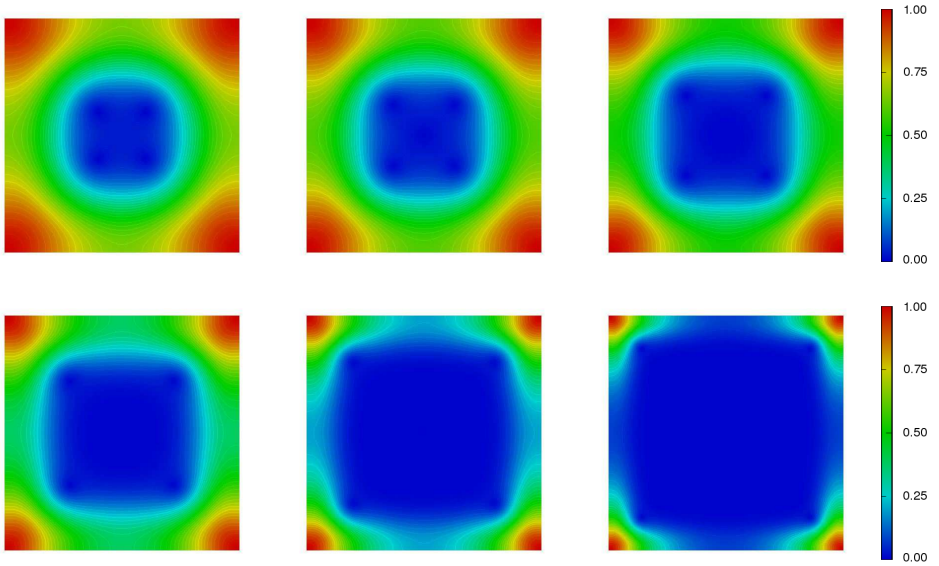

Figure 6: Moduli of the first eigenfunction, $h = 0.1,\ 0.08,\ 0.06,\ 0.04,\ 0.02,\ 0.01$.

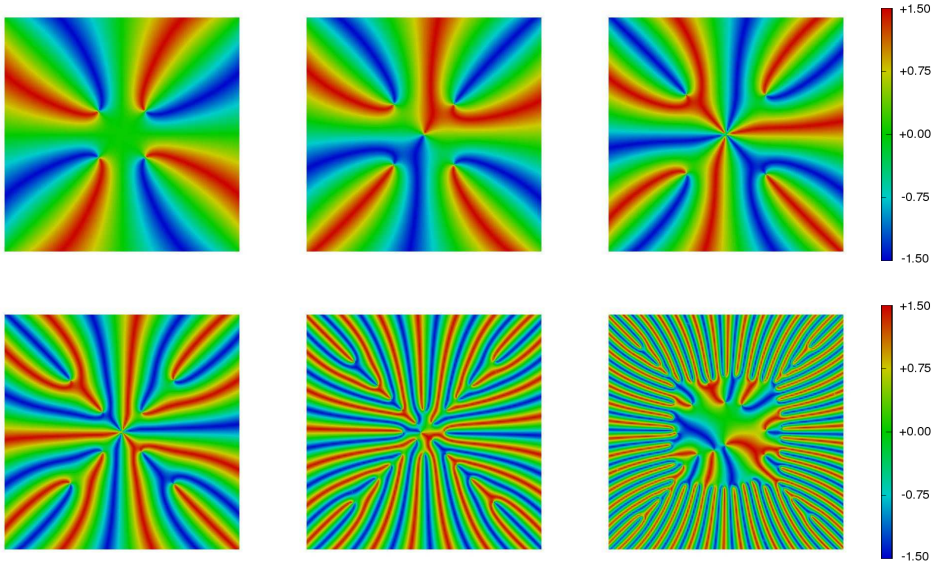

Figure 7: Phases of the first eigenfunction, $h = 0.1,\ 0.08,\ 0.06,\ 0.04,\ 0.02,\ 0.01$.

4.3 Dependency on the rank of eigenfunctions for a given value of h

In Figures 8 we keep $h = 0.02$ fixed and compute the eigenfunctions associated with the smallest eight eigenvalues of P_h. We observe that the eigenvectors associated with the smallest four eigenvalues are localized in the four corners as predicted by Proposition 4.2, and that, moreover, each one is present in all the four corners, as can be predicted by symme-

try arguments. There is no theoretical results for the next eigenpairs, but the computations show a localization of the eigenvectors along the edges of the square.

The full portrait (modulus and phase) of the first 32 modes can be found in Appendix A.

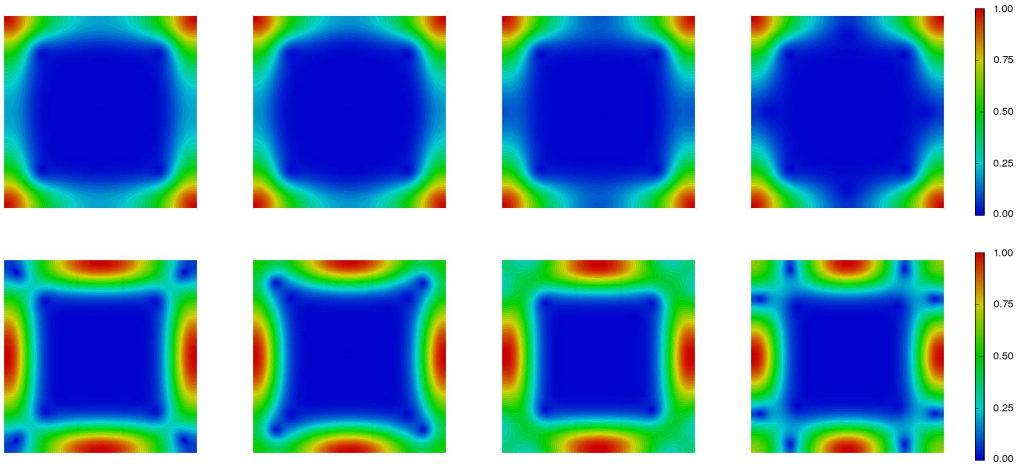

Figure 8: Moduli of the first 8 eigenfunctions, $h = 0.02$.

4.4 Tunneling effect

The *tunneling effect* refers to the interaction between symmetric potential wells, see [21] for instance. In our situation, the tunneling effect applies to corners of the same aperture. If present, this effect is an interaction of eigenvalues inside the same cluster, possibly stronger than the convergence of the whole cluster to its asymptotic limit. It could be formally evaluated by investigating the eigenpairs of the Galerkin projection on the space of quasi-modes $\breve{\psi}_{h,\mathsf{s}_j}$.

Here, we simply compute, not only the first 4, but the first 12 eigenvalues, with a $\mathbb{Q}_{10}$-approximation on uniform meshes of 4 to 64 elements, according to the value of $1/h$, ranging from 1 to 90, with step 0.5. We present in Figure 9 the graph of these first 12 eigenvalues divided by h, vs. h^{-1}. We observe that the eigenvalues interlace inside clusters of four. The first cluster, converging to the value $\mu_1(\pi/2) \simeq 0.5099$, is contained in an *exponential tube* (materialized in the figure by the dashed curves of equation $h^{-1} \mapsto 0.5099 \pm 0.6 \exp(-0.5665\, h^{-1/2})$ as a numerical representation of the asymptotics (10)). The further clusters remain higher than $\Theta_0 \simeq 0.59$.

We note that, since P_h is self-adjoint and its coefficients depend analytically on h, its eigenvalues can be organized to display an *analytic* dependence on h in any interval disjoint from 0. By a simple automatic postprocessing of the results, we follow eigenvalues as *families depending smoothly on* h.

The multiple crossings between eigenvalues are corroborated by a closer look at the eigenvectors: Tracking the symmetry properties of eigenvectors, it becomes obvious that the crossings really occur. These oscillations are due to the magnetic field, and do not exist in presence of an electric field alone.

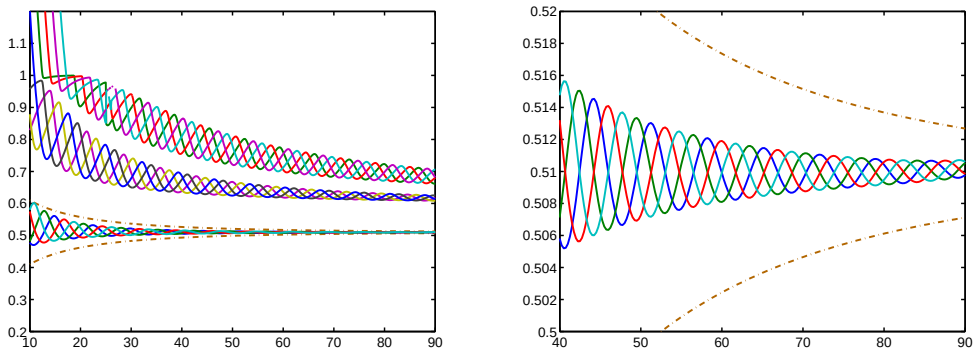

Figure 9: $h^{-1}\mu_{h,n}$ vs. h^{-1}, $n = 1, \ldots, 12$ in Ω_{sq} (left). Zoom to the first cluster (right).

5 Other polygons

Let now Ω denote a general polygon with straight edges. The behavior of the lowest eigenvalues of the Neumann realization P_h of the operator $-(h\nabla - i\mathcal{A})^2$ on Ω as h tends to 0 has, in a certain sense, the same features as previously.

Let Σ be the set of the vertices s of Ω, and α_{s} be the opening of Ω at the vertex s. As already seen in the case of the square, the spectrum of P_h is in close relation with the spectra of the model operators $Q^{\alpha_{\mathsf{s}}}$ for s describing the set of corners Σ.

5.1 Theoretical results

Let us suppose for sake of simplicity that, for any vertex s, the model operator $Q^{\alpha_{\mathsf{s}}}$ has at most one eigenvalue $\mu_1(\alpha_{\mathsf{s}})$. This is the case for the examples we propose. From previous computations, see Remark 3.3, it is enough that the openings α_{s} are greater than $\pi/5$. See [10] for the general case.

Let Σ_1 be the set of vertices s such that $\mu_1(\alpha_{\mathsf{s}}) < \Theta_0$. From Remark 3.3 again, Σ_1 coincides with the set of convex vertices of Ω.

Notation 5.1. • Let $\mu_{h,n}$ be the n-th eigenvalue of P_h counted with multiplicity.
• Let λ_n be the n-th element of the set $\{\mu_1(\alpha_{\mathsf{s}}),\ \mathsf{s} \in \Sigma_1\}$.
• Let ρ be the minimum distance between two corners of Ω.

Theorem 5.2. *With Notation* 5.1*, for any $\varepsilon > 0$, there exists C_ε such that*

$$|\mu_{h,n} - h\lambda_n| \leq C_\varepsilon \exp\left(-\frac{1}{\sqrt{h}}\left(\rho\sqrt{\Theta_0 - \lambda_n} - \varepsilon\right)\right), \quad \forall n \leq N := \#(\Sigma_1).$$

Thus, according to repetitions of the same value λ in $\{\lambda_1, \ldots, \lambda_N\}$, the corresponding eigenvalues $\mu_{h,n}$ are gathered into clusters, exponentially close to the same value $h\lambda$. It is proved in [10] that the corresponding eigenvectors are exponentially close to linear combinations of quasi-modes: Quasi-modes $\psi_{h,\mathsf{s}}$ are defined by translation, rotation, scaling, and

cut-off from the eigenvectors $\Psi_1^{\alpha_\mathsf{s}}$ for any $\mathsf{s} \in \Sigma_1$ like in Notation 4.1 for the square,

$$\psi_{h,\mathsf{s}}(x) \;=\; \chi_\mathsf{s}(x)\,\frac{1}{\sqrt{h}}\exp\left(\frac{i}{2h}\,x\wedge\mathsf{s}\right)\;\Psi_1^{\alpha_\mathsf{s}}\left(\frac{\mathcal{R}_\mathsf{s}(x-\mathsf{s})}{\sqrt{h}}\right).$$

Notation 5.3. • Using Notation 5.1, we denote by $\{\Lambda_1 < \cdots < \Lambda_M\}$ the set of distinct values in $\{\lambda_1, \ldots, \lambda_N\}$.

• For any $m \leq M$, we define the m-th cluster of eigenspaces of P_h by

$$F_{h,m} = \mathrm{span}\big\{u_{h,n} \mid \forall n \;\text{ such that }\; \lambda_n = \Lambda_m\big\},$$

and the corresponding cluster $F_{h,m}$ of quasi-modes

$$E_{h,m} = \mathrm{span}\big\{\psi_{h,\mathsf{s}} \mid \forall \mathsf{s} \in \Sigma_1 \;\text{ such that }\; \mu_1(\alpha_\mathsf{s}) = \Lambda_m\big\}.$$

Theorem 5.4. *For any $\varepsilon \geq \delta$, with δ depending on the cut-off functions χ_s, there exists $C_\varepsilon > 0$ such that for any $m \leq M$,*

$$d(E_{h,m}\,, F_{h,m}) \leq C_\varepsilon \exp\left(-\frac{1}{\sqrt{h}}\left(\rho\sqrt{\Theta_0 - \Lambda_m} - \varepsilon\right)\right).$$

5.2 Rhombus and Trapezoid

We consider two examples of convex quadrilateral domains, a rhombus Ω_rh with two pairs of distinct openings, and a trapezoid Ω_tr without symmetry with two openings equal.

The corners of the rhombus Ω_rh are $\mathsf{s}_1 = (-\sqrt{2}/2, 0)$, $\mathsf{s}_2 = (0, -\sqrt{2})$, $\mathsf{s}_3 = (\sqrt{2}/2, 0)$, $\mathsf{s}_4 = (0, \sqrt{2})$. As illustrated in Figure 10, for $h = 0.02$ the first two eigenvectors are localized in the smallest openings, whereas the third and the fourth one are localized in the largest openings. Because of symmetry, these eigenvectors are localized in two corners and not in one only.

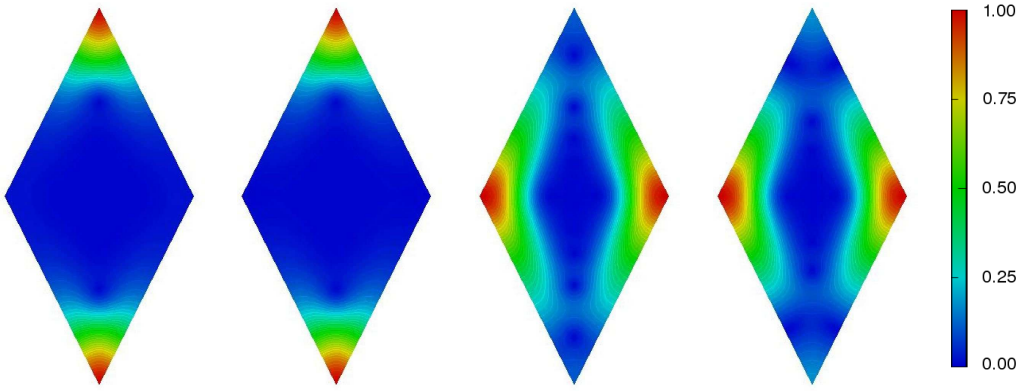

Figure 10: Moduli of eigenvectors 1 to 4 in Ω_rh for $h = 0.02$.

The corners of the trapezoid Ω_tr are $\mathsf{s}_1 = (-1, -1)$, $\mathsf{s}_2 = (1, -1)$, $\mathsf{s}_3 = (1, 0)$, $\mathsf{s}_4 = (-1, 1)$. Thus the openings at s_1 and s_2 are equal to $\pi/2$. We show in Figure 11 the

first four eigenvectors for $h = 0.02$. As expected, the corners are visited according to increasing magnitude. An interesting difference from the symmetric case is the localization of eigenvectors 2 and 3 in corners s_1 and s_2 with quite different coefficients. We have noticed that the concentration in one corner only is stronger as h gets smaller. The pictures of moduli in log10 scale (bottom) give another insight on the support of eigenvectors.

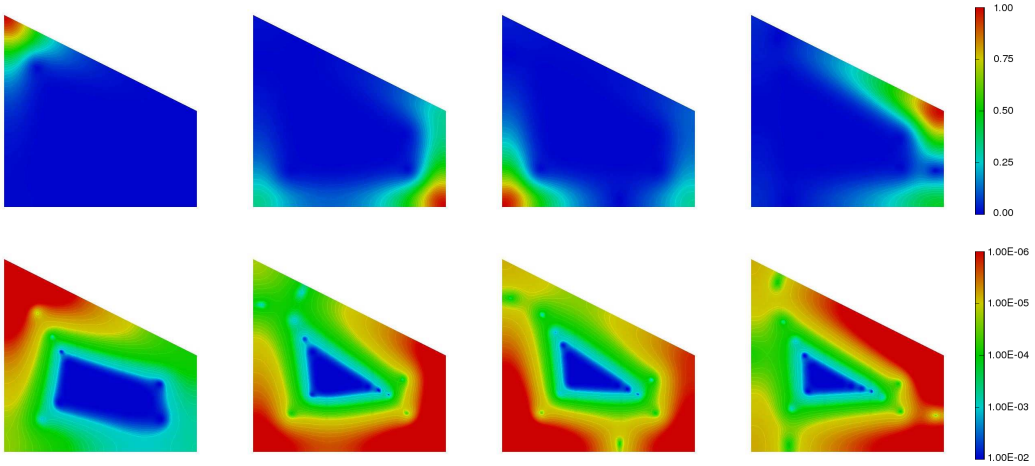

Figure 11: Moduli of eigenvectors 1 to 4 in Ω_{tr} for $h = 0.02$.
Natural color scale (top) and logarithmic color scale (bottom)

The plots of $h^{-1}\mu_{h,n}$ vs. h^{-1} display two convergent two-element clusters for the rhombus (note the values of $\mu_1(\alpha)$ estimated by the method in §3 for the two different openings: 0.395 and 0.565), and three distinct limits for the trapezoid (note: $\mu_1(\alpha) \simeq 0.434$, 0.510 and 0.554). Eigenvalues interlace much less in the trapezoid, because of the absence of symmetry.

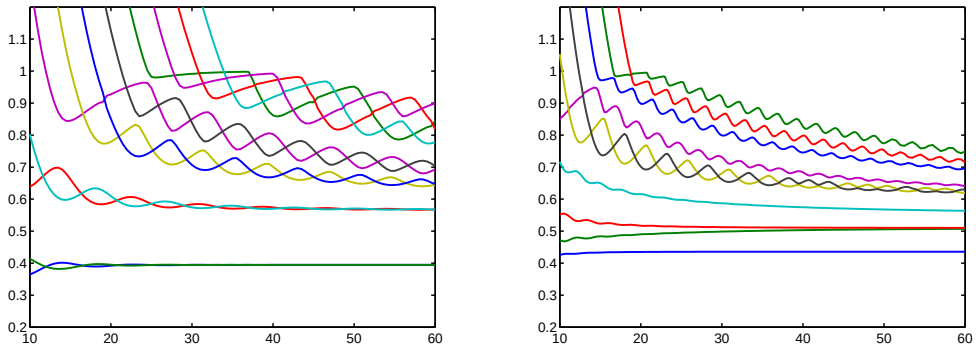

Figure 12: $h^{-1}\mu_{h,n}$ vs. h^{-1} for Ω_{rh} (left) and Ω_{tr} (right).

5.3 L-shape

The L-shaped domain Ω_{L} has six corners: $\mathsf{s}_1 = (0,0)$, $\mathsf{s}_2 = (2,0)$, $\mathsf{s}_3 = (2,1)$, $\mathsf{s}_4 = (1,1)$, $\mathsf{s}_5 = (1,2)$, $\mathsf{s}_6 = (0,2)$. Thus it has 5 corners of same opening $\pi/2$ and one non-convex corner. The big five element cluster around $\mu_1(\pi/2)$ splits in fact in three sub-clusters of 2, 1 and 2 elements, respectively, see Figure 14.

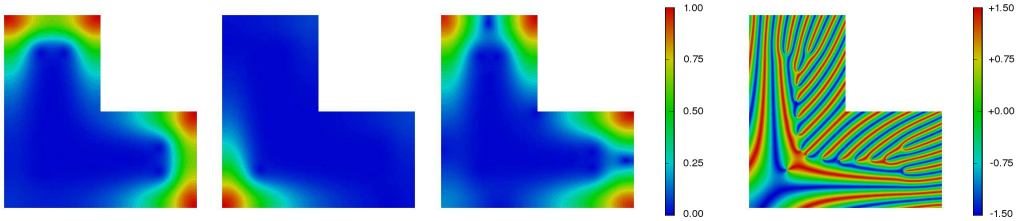

Figure 13: Moduli of eigenvectors 1, 3 and 5 in Ω_{L}, phase of eigenvector 1.

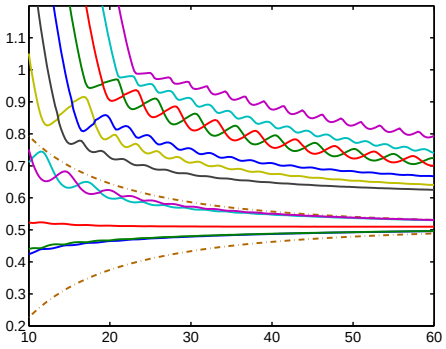

Figure 14: $h^{-1}\mu_{h,n}$ vs. h^{-1} for the L-shape Ω_{L}.

6 Curvilinear polygonal domains

If Ω is a curvilinear polygon, as proved in [10], we still have convergence of the eigenpairs of P_h towards those of $\oplus_{\mathsf{s}\in\Sigma_1} Q^{\alpha_{\mathsf{s}}}$, but instead of being exponential, the convergence has the rate $\sqrt{h}$. Nevertheless, clustering and tunnelling are still present if the domain is symmetric, as shown on the curved square Ω_{curv} below. The opening of the angles of Ω_{curv} is equal to 0.650π, corresponding to $\mu_1(\alpha) = 0.554$. A geometrical interpolation of degree 4 has been used for the design of the 8×8 mesh.

From Figure 16, the slower convergence and weaker concentration of eigenvalues inside their cluster are visible, when compared to the case of the square (see Figure 9).

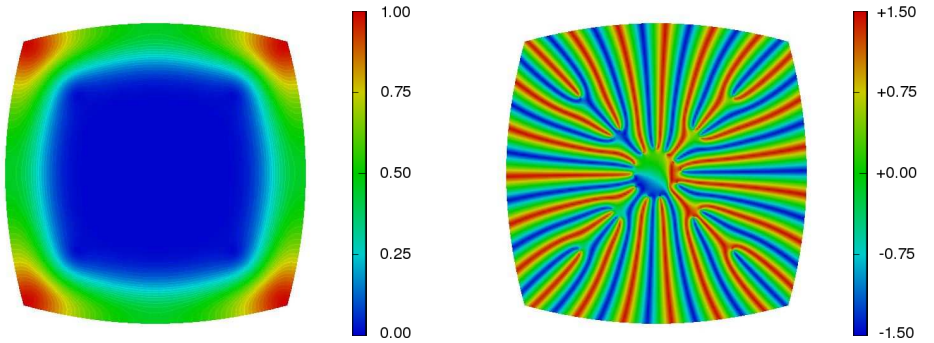

Figure 15: First eigenvector on the curved square Ω_{curv} (modulus and phase).

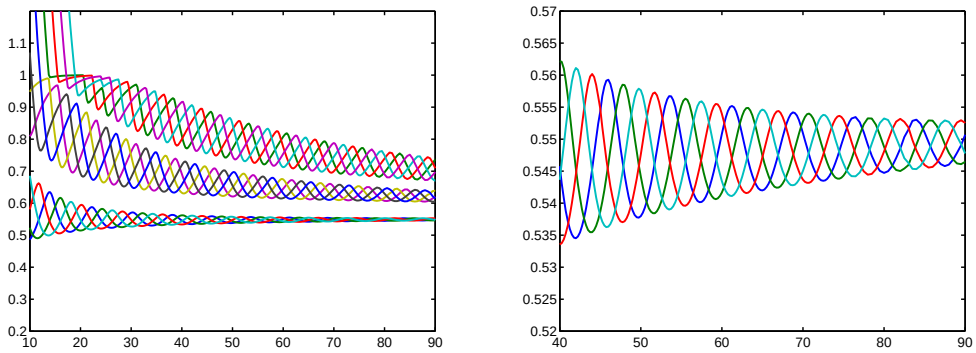

Figure 16: $h^{-1}\mu_{h,n}$ vs. h^{-1}, $n = 1, \ldots, 12$, in the curved square Ω_{curv}.

7 h-extension vs. p-extension

We now compare in a systematic way the performances of the h-extension (i.e. keep the polynomial degree fixed and refine the mesh) with those of the p-extension (i.e. keep the mesh fixed and increase the polynomial degree). All numerical experiments are carried with the standard square Ω_{sq} centered at $(0, 0)$ with side length 2.

In §7.1 we keep the number of degrees of freedom (Dof) equal to 1600 and compare the dependency on the small parameter h of eigenvalues computed with different combinations of meshes and degrees. In §7.2 and §7.3 the parameter h is set to 0.02 and show errors for h- and p-extensions, respectively.

7.1 Several combinations mesh-degree

We compute the first eight eigenvalues of P_h on the square Ω_{sq} for $h^{-1} = 10$ to 60 by step 0.5 with four different combinations of 1600 Dof: $\mathbb{Q}_1$ in a 40×40 mesh, $\mathbb{Q}_2$ in a 20×20 mesh, $\mathbb{Q}_5$ in a 8×8 mesh, and, finally, $\mathbb{Q}_{20}$ in a 2×2 mesh. We plot in Figures 17

the first eight discrete eigenvalues divided by h, vs. h^{-1}, and according to their smooth dependency in h (like for Figure 9). And, like in Figure 9, for the same reason, we plot in dashed lines the exponential tube $h^{-1} \mapsto 0.5099 \pm 0.6\exp(-0.5665\,h^{-1/2})$. We recall that we expect the first four eigenvalue cluster to concentrate inside this tube.

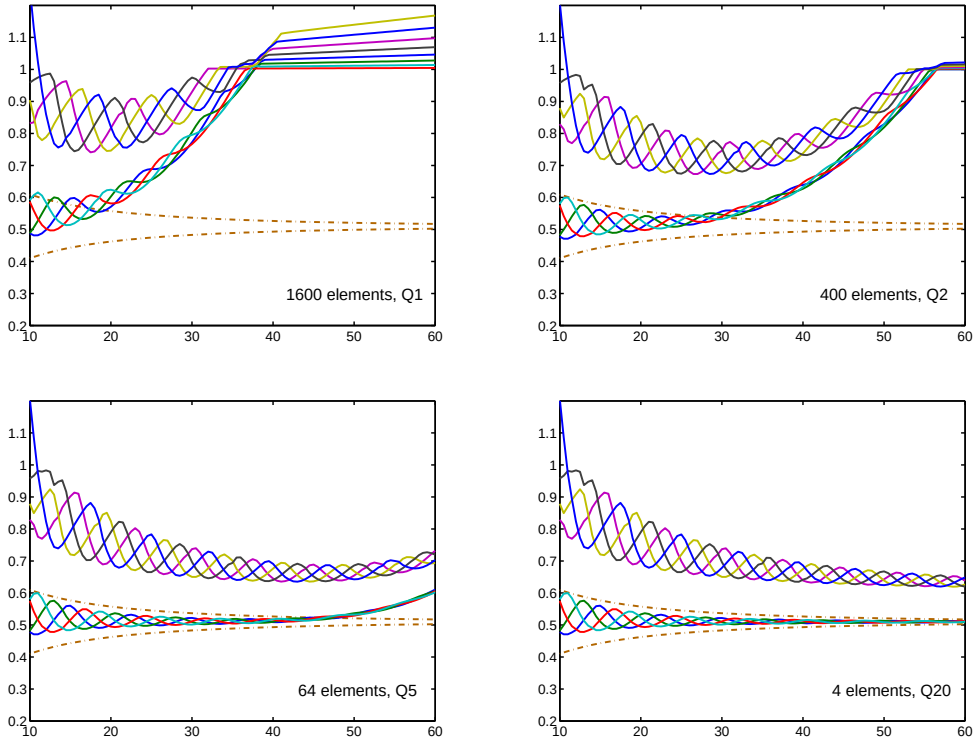

Figure 17: $h^{-1}\mu_{h,n}$ vs. h^{-1} for 1600 Dof

Besides the clearly visible better performance of high degree, two features are noticeable: *(i)* While they are below 1, the eight eigenvalues still gather into two clusters and interlace with each other, and *(ii)* when eigenvalues get higher than 1, they stick to this value and do not oscillate any more.

7.2 h-extension with degree 1 and 2

The semi-classical parameter h is fixed to 0.02. The reference value is taken to 0.50726621 for $h^{-1}\mu_{h,1}$, and is obtained with $\mathbb{Q}_{12}$-approximation on the 8×8 mesh.

From Figure 18, we observe a preasymptotic convergence to 1, followed by the asymptotic convergence towards $h^{-1}\mu_{h,1}$. The preasymptotic convergence appears to be faster. A closer look at the log-log plots of Figure 19 shows that the convergence *rates* are similar: If ℓ denotes the mesh size, the rates are approximately ℓ^2 and ℓ^4 for $\mathbb{Q}_1$ and $\mathbb{Q}_2$, respectively, but the errors behave like $C\ell^2$ and $C\ell^4$ with a much larger C for the asymptotic convergence than for the preasymptotic one.

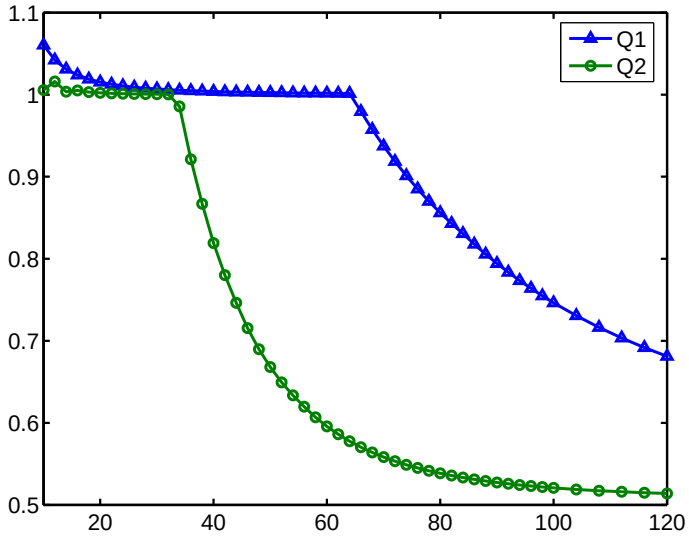

Figure 18: $h^{-1}\mu_{h,1}$ vs. number of Dof per side for $\mathbb{Q}_1$ and $\mathbb{Q}_2$-approximation.

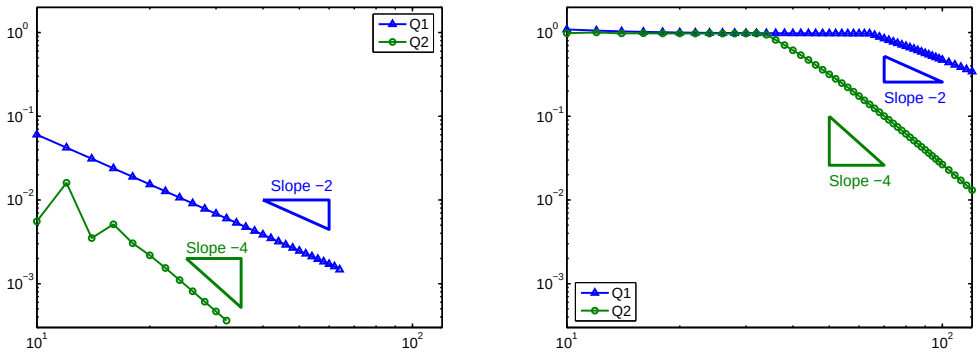

Figure 19: Relative errors for first eigenvalue, vs. number of Dof per side.
Errors wrt preasymptotic value 1 *(left), and to exact value* 0.50726621 *(right)*

The structure of theses results evokes a possible crossing between two very different modes. We display the portrait (modulus and phase) of the first eight eigenvectors computed with a $\mathbb{Q}_1$-approximation on a 63×63 mesh (i.e., the last one before the bifurcation point of the $\mathbb{Q}_1$ curve, cf. Figure 18).

It is clear that modes 1, 2, 3, 5 and 8 are of different nature, and that modes 4, 6 and 7 are somewhat closer to "true" modes 5-8, see Figure 8. These less oscillating modes, especially 1-3, look like the first *Landau modes*

$$(\mathsf{X}_1, \mathsf{X}_2) \longmapsto (\mathsf{X}_1 + i\mathsf{X}_2)^n \exp\Big(-\frac{1}{4}(\mathsf{X}_1^2 + \mathsf{X}_2^2)\Big),$$

for $n = 0, 1, 2$ and the scaling $\mathsf{X} = \frac{x}{\sqrt{h}}$. The Landau modes are a basis of the (infinite

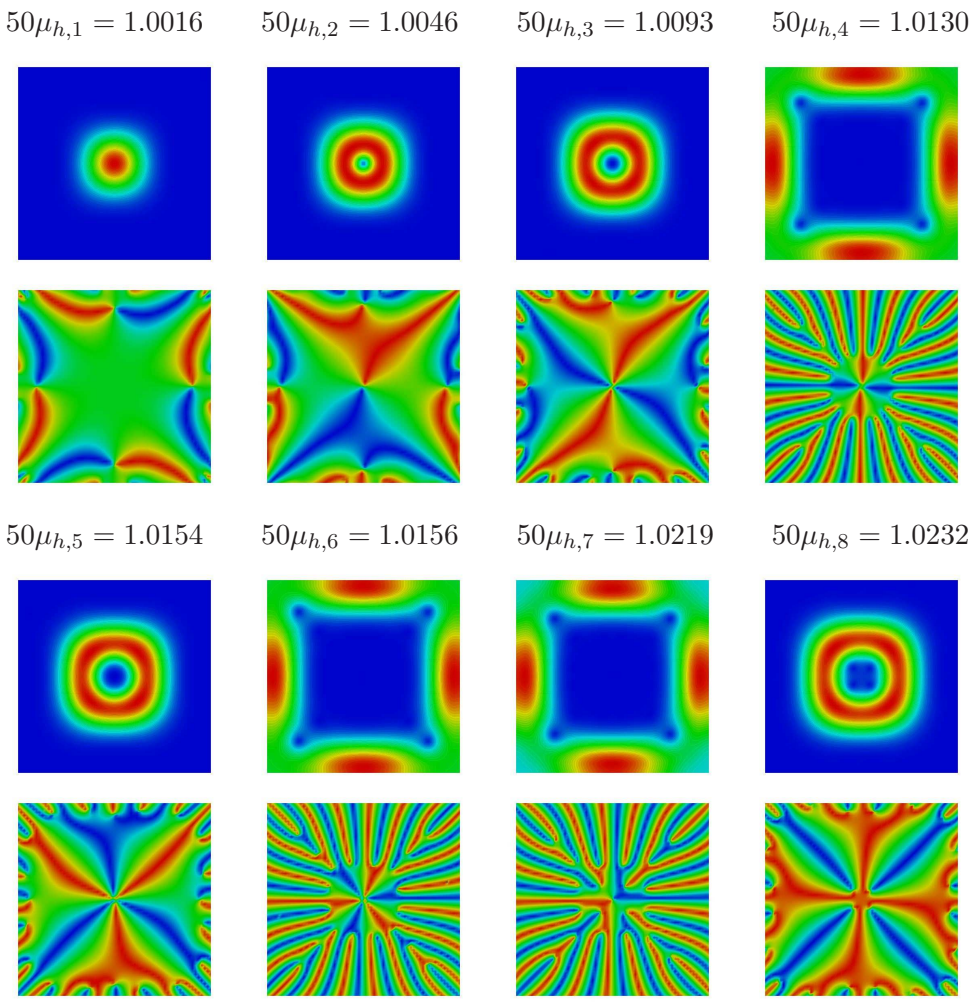

Figure 20: Modes 1 to 8, $h = 0.02$, $\mathbb{Q}_1$-approximation on 63×63 mesh.
Moduli (top) and phases (bottom)

dimensional) eigenspace of the operator $-(\nabla - i\mathcal{A})^2$ in $\mathbb{R}^2$, for the *lowest Landau level*, that is, 1.

Examining the sequence of the first 32 modes computed with the $\mathbb{Q}_{10}$-approximation on the 8×8 mesh, we can see that some of them, especially 32, 31 and 30, also look like the first three Landau modes (cf. Appendix A).

From the 63×63 mesh to the 64×64 mesh, we do observe crossings between modes: For instance mode 4 becomes mode 1. Besides, the structure of oscillating modes 4, 6 ad 7 produced with the 63×63 mesh is very close to that of exact modes.

7.3 p-extension with coarse meshes

As in the previous section, the semi-classical parameter h is fixed to 0.02 and the reference value is the same.

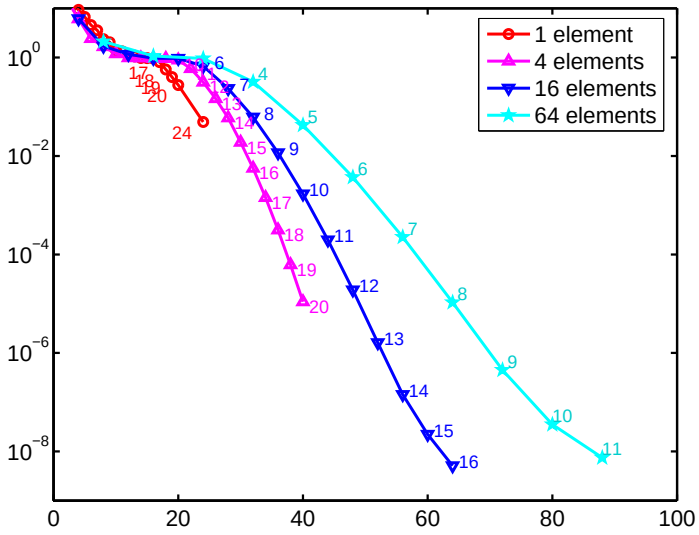

Figure 21: Relative errors for first eigenvalue, vs. number of Dof per side.
Semi-logarithmic scale from 10^{-9} *to* 10 *for errors. Integers mark polynomial degree.*

We plot on separate curves the errors for each mesh, letting the degree vary. We still notice a locking region, where $h^{-1}\mu_{h,1}$ converges to 1 (which also corresponds to a relative error $\simeq 1$). This region expands with the number of elements of the mesh. But, as a result, with the same number of Dof the p-extension is far more precise than the h-extension.

8 Conclusion

Even with a size ratio equal to 100 between the domain Ω and the semi-classical parameter h (this is the case for Ω_{sq} with $h = 0.02$), the computation of the eigenpairs of P_h is a numerical challenge for two reasons: *(i)* the double scale for the first eigenvectors, inducing oscillations of wave length $\mathcal{O}(h)$,[2] *(ii)* the presence of different asymptotic modes, possibly less oscillatory, like the Landau modes.

In fact, depending on the position of the domain with respect to the gauge center, the preasymptotic convergence will have quite different features: For a small enough h fixed like in the previous section, decreasing the mesh size with a low degree approximation provides a preasymptotic concentration of the first mode around the gauge center. This phenomenon has been observed in [25], too. Thus it is very useful to know the asymptotic

[2]The somewhat odd fact that the first mode is increasingly oscillating as $h \to 0$ has some similarity with the situation of sensitive shells, see [12].

behavior of eigenmodes before trying to compute them. This prevents to believe that the first mode is approached as soon as a convergence appears.

From a more theoretical point of view, this rather simple, but very rich, example proves the importance and the role of the global constant $L_{h,n}^{\ell,p}$ in estimates (1) and (2). The capability of approximating the first mode of the continuous problem is *not sufficient* for a precise computation of its first eigenpair, cf. Figure 20. In other words, we do not have the strict analogue of Céa lemma for eigenpair approximation. Nevertheless, the obvious better performances of p-extension over h-extension have some connection to the approximability of oscillatory functions by high degree polynomials, better than by piecewise affine or quadratic functions.

As a last remark, we notice the absence of influence of corner singularities for this problem: *(i)* eigenmodes are mainly supported outside non-convex corners and *(ii)* the effect of singularities at convex corners will be felt after the oscillations are resolved (beyond a relative error of 10^{-6} in Figure 21). The main role played by these oscillations, and the fact that they spread everywhere in the domain makes it useless to refine meshes near corners. On the contrary, *uniform* meshes have provided the most precise results regarding fine interactions between corners (the tunnelling effect).

References

[1] AINSWORTH, M. Discrete dispersion relation for hp-version finite element approximation at high wave number. *SIAM J. Numer. Anal. 42*, 2 (2004), 553–575 (electronic).

[2] ALMOG, Y. The onset of superconductivity in long rectangles. *European J. Appl. Math. 14*, 3 (2003), 257–277.

[3] ALOUGES, F., AND BONNAILLIE-NOËL, V. Numerical computations of fundamental eigenstates for the Schrödinger operator under constant magnetic field. *To appear in Numerical Methods for PDE* (2005).

[4] BABUŠKA, I., AND OSBORN, J. E. Finite element-Galerkin approximation of the eigenvalues and eigenvectors of self-adjoint problems. *Math. Comp.*, 186 (1989), 275–297.

[5] BABUŠKA, I., AND OSBORN, J. E. *Eigenvalue problems*, vol. 2. Handbook of numerical analysis, 1991.

[6] BAUMAN, P., PHILLIPS, D., AND TANG, Q. Stable nucleation for the Ginzburg-Landau system with an applied magnetic field. *Arch. Rational Mech. Anal. 142*, 1 (1998), 1–43.

[7] BERNOFF, A., AND STERNBERG, P. Onset of superconductivity in decreasing fields for general domains. *J. Math. Phys. 39*, 3 (1998), 1272–1284.

[8] BONNAILLIE, V. On the fundamental state energy for a Schrödinger operator with magnetic field in domains with corners. *Asymptot. Anal. 41*, 3-4 (2005), 215–258.

[9] BONNAILLIE-NOËL, V. A posteriori error estimator for the eigenvalue problem associated to the Schrödinger operator with magnetic field. *Numer. Math. 99*, 2 (2004), 325–348.

[10] BONNAILLIE-NOËL, V., AND DAUGE, M. Asymptotics for the low-lying eigenstates of the Schrödinger operator with magnetic field near corners. *Preprint IRMAR 05-27* (2005).

[11] CHATELIN, F. *Spectral Approximations of Linear operators*. Academic Press, New York, 1983.

[12] DAUGE, M., FAOU, E., AND YOSIBASH, Z. Plates and shells: Asymptotic expansions and hierarchical models. In *Encyclodepia of Computational Mechanics, Vol. 1*, E. Stein, R. de Borst, and T. J. Hughes, Eds. Wiley, 2004, pp. 199–236.

[13] DE GENNES, P. G. *Superconductivity in metals and Alloys*. Addison Wesley, 1989.

[14] DEL PINO, M., FELMER, P. L., AND STERNBERG, P. Boundary concentration for eigenvalue problems related to the onset of superconductivity. *Comm. Math. Phys. 210*, 2 (2000), 413–446.

[15] FOURNAIS, S., AND HELFFER, B. Accurate eigenvalue estimates for the magnetic Neumann Laplacian. *To appear in Annales Inst. Fourier* (2005).

[16] FOURNAIS, S., AND HELFFER, B. Energy asymptotics for type II superconductors. *Calc. Var. 24*, 3 (2005), 341–376.

[17] FOURNAIS, S., AND HELFFER, B. On the third critical field in Ginzburg-Landau theory. *Preprint Orsay 2005-37* (2005).

[18] HELFFER, B., AND MOHAMED, A. Semiclassical analysis for the ground state energy of a Schrödinger operator with magnetic wells. *J. Funct. Anal. 138*, 1 (1996), 40–81.

[19] HELFFER, B., AND MORAME, A. Magnetic bottles in connection with superconductivity. *J. Funct. Anal. 185*, 2 (2001), 604–680.

[20] HELFFER, B., AND PAN, X.-B. Upper critical field and location of surface nucleation of superconductivity. *Ann. Inst. H. Poincaré Anal. Non Linéaire 20*, 1 (2003), 145–181.

[21] HELFFER, B., AND SJÖSTRAND, J. Multiple wells in the semiclassical limit. I. *Comm. Partial Differential Equations 9*, 4 (1984), 337–408.

[22] IHLENBURG, F., AND BABUŠKA, I. Finite element solution of the Helmholtz equation with high wave number. I. The h-version of the FEM. *Comput. Math. Appl. 30*, 9 (1995), 9–37.

[23] IHLENBURG, F., AND BABUŠKA, I. Finite element solution of the Helmholtz equation with high wave number. II. The h-p version of the FEM. *SIAM J. Numer. Anal. 34*, 1 (1997), 315–358.

[24] JADALLAH, H. T. The onset of superconductivity in a domain with a corner. *J. Math. Phys. 42*, 9 (2001), 4101–4121.

[25] JANANE, R. *Études numériques du spectre d'un opérateur de Schrödinger avec champ magnétique constant*. Thèse de doctorat, Université de Nantes, 2005.

[26] LU, K., AND PAN, X.-B. Estimates of the upper critical field for the Ginzburg-Landau equations of superconductivity. *Phys. D 127*, 1-2 (1999), 73–104.

[27] MARTIN, D. The finite element library Mélina. http://perso.univ-rennes1.fr/daniel.martin/melina (2005).

[28] PAN, X.-B. Upper critical field for superconductors with edges and corners. *Calc. Var. Partial Differential Equations 14*, 4 (2002), 447–482.

[29] TINKHAM, M. *Introduction to superconductivity*. McGraw Hill, 1996.

Authors' address

IRMAR (UMR CNRS 6625)
Université de Rennes 1,
Campus de Beaulieu
35042 RENNES Cedex
FRANCE

Corresponding author
Monique Dauge, monique.dauge@univ-rennes1.fr

Appendix A: The first 32 eigenpairs in the square for $h = 0.02$.

Computed in Ω_{sq} with the $\mathbb{Q}_{10}$-approximation on the 8×8 mesh.

We give, for each computed eigenmode, its rank n, the value of $h^{-1}\mu_{h,n}$, the modulus and the phase of a normalized eigenvector.

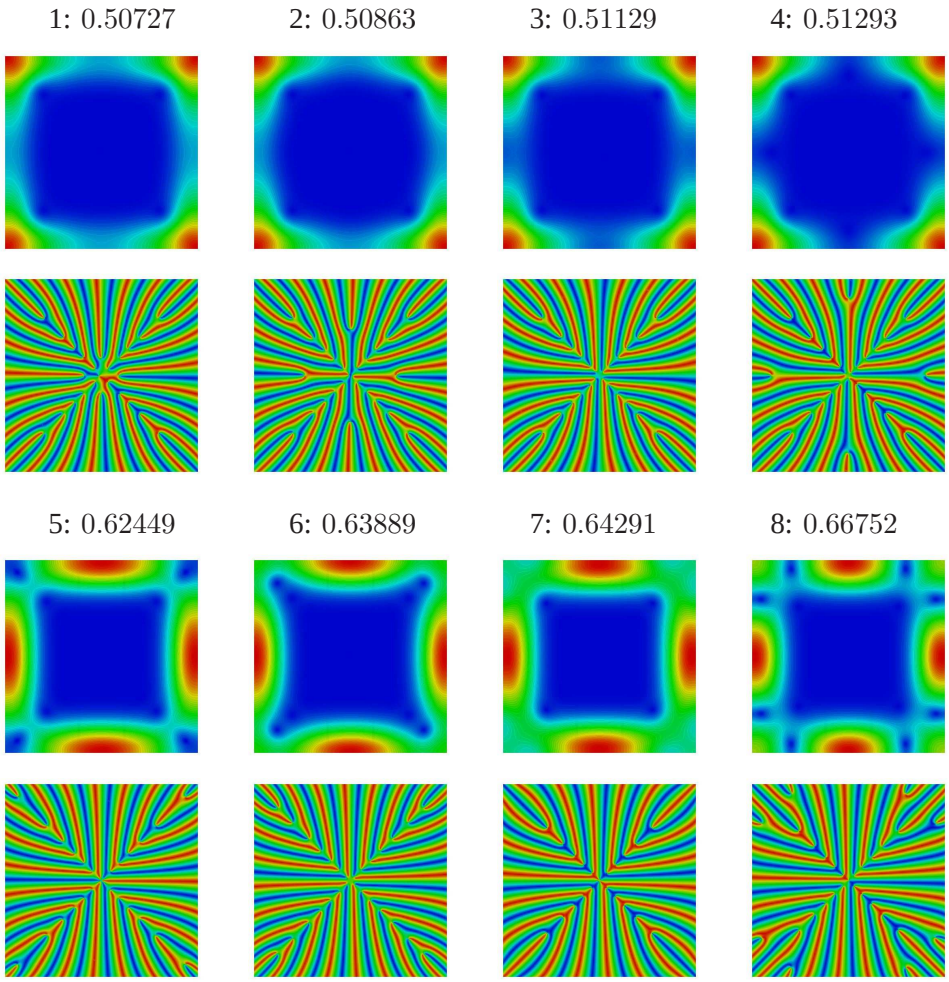

Figure 22: Modes 1 to 8, Modulus (top) and phase (bottom).

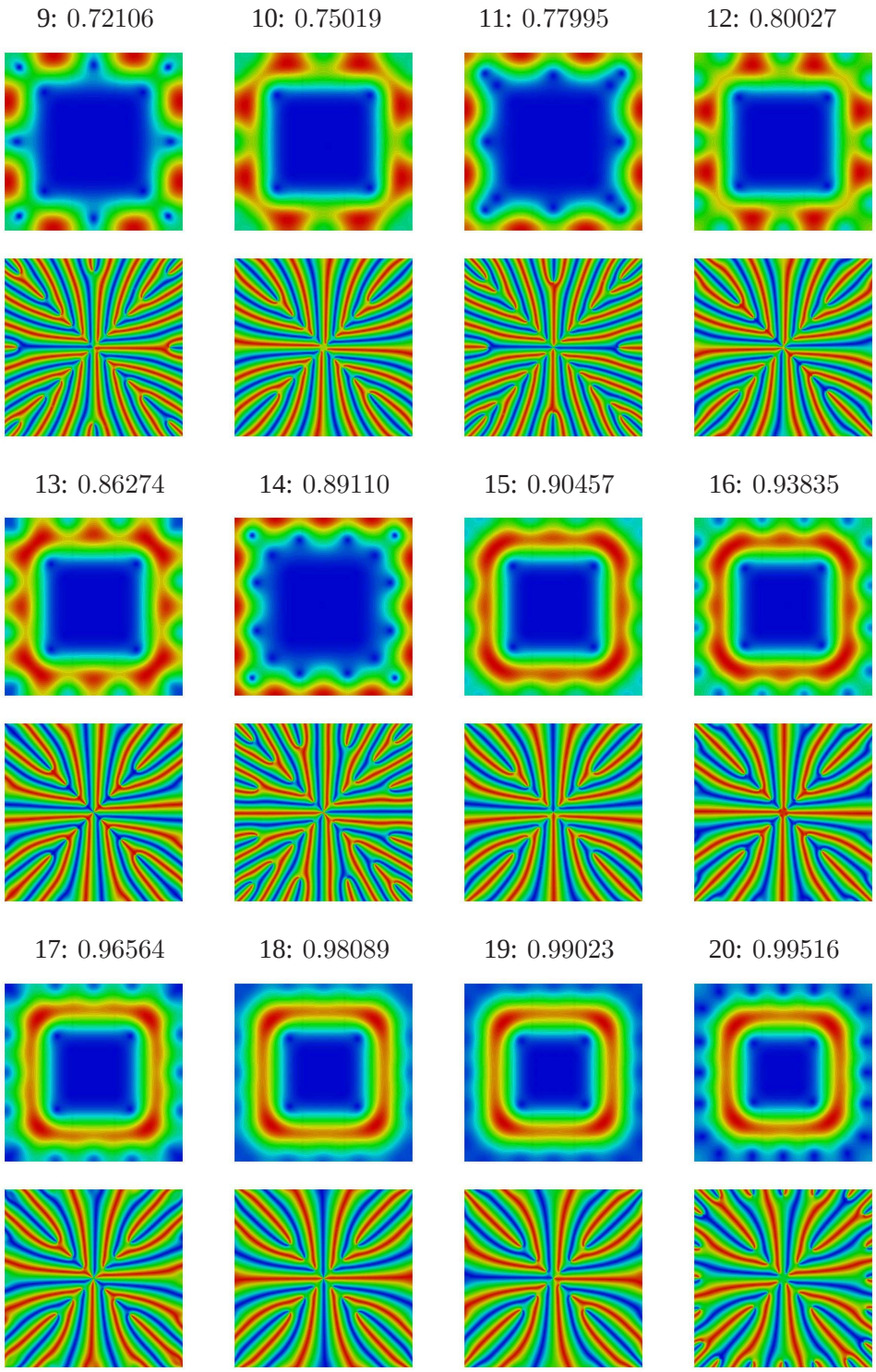

Figure 23: Modes 9 to 20, Modulus (top) and phase (bottom).

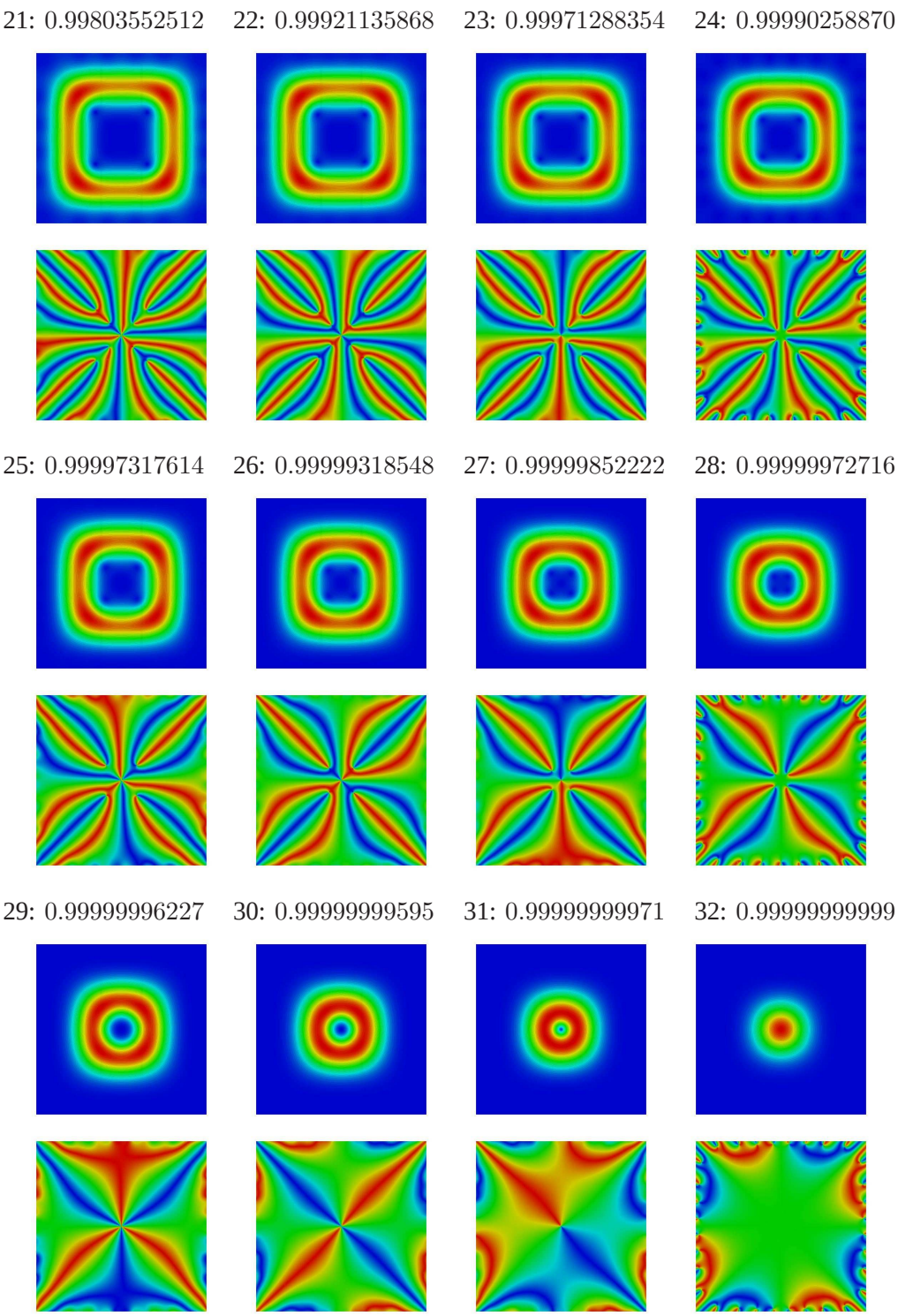

Figure 24: Modes 21 to 32, Modulus (top) and phase (bottom).

Appendix B: Table of $\mu_1(\alpha)$ vs. α

In the next two tables, in each column the integer number j determines α by $\alpha = j\pi/1000$, the real number besides is $\mu_1(\alpha)$.

1	0.0018138	41	0.073586	81	0.14141	121	0.20305	161	0.25773
2	0.0036275	42	0.075342	82	0.14303	122	0.2045	162	0.25901
3	0.0054411	43	0.077096	83	0.14465	123	0.20595	163	0.26029
4	0.0072544	44	0.078848	84	0.14627	124	0.20739	164	0.26155
5	0.0090675	45	0.080597	85	0.14788	125	0.20883	165	0.26282
6	0.01088	46	0.082343	86	0.14948	126	0.21027	166	0.26408
7	0.012693	47	0.084086	87	0.15108	127	0.2117	167	0.26534
8	0.014504	48	0.085826	88	0.15268	128	0.21313	168	0.26659
9	0.016316	49	0.087564	89	0.15428	129	0.21455	169	0.26784
10	0.018126	50	0.089298	90	0.15587	130	0.21597	170	0.26908
11	0.019936	51	0.09103	91	0.15745	131	0.21738	171	0.27032
12	0.021745	52	0.092758	92	0.15903	132	0.21879	172	0.27156
13	0.023554	53	0.094484	93	0.16061	133	0.22019	173	0.27279
14	0.025361	54	0.096206	94	0.16218	134	0.22159	174	0.27401
15	0.027168	55	0.097926	95	0.16375	135	0.22299	175	0.27524
16	0.028973	56	0.099642	96	0.16532	136	0.22438	176	0.27645
17	0.030777	57	0.10135	97	0.16688	137	0.22576	177	0.27767
18	0.03258	58	0.10306	98	0.16843	138	0.22715	178	0.27888
19	0.034382	59	0.10477	99	0.16999	139	0.22852	179	0.28009
20	0.036183	60	0.10647	100	0.17153	140	0.2299	180	0.28129
21	0.037982	61	0.10817	101	0.17308	141	0.23127	181	0.28248
22	0.03978	62	0.10987	102	0.17462	142	0.23263	182	0.28368
23	0.041576	63	0.11156	103	0.17615	143	0.23399	183	0.28487
24	0.043371	64	0.11325	104	0.17768	144	0.23535	184	0.28605
25	0.045164	65	0.11494	105	0.17921	145	0.2367	185	0.28723
26	0.046955	66	0.11662	106	0.18073	146	0.23805	186	0.28841
27	0.048745	67	0.1183	107	0.18225	147	0.23939	187	0.28958
28	0.050533	68	0.11997	108	0.18377	148	0.24073	188	0.29075
29	0.052319	69	0.12164	109	0.18527	149	0.24206	189	0.29192
30	0.054103	70	0.12331	110	0.18678	150	0.24339	190	0.29308
31	0.055885	71	0.12498	111	0.18828	151	0.24472	191	0.29424
32	0.057665	72	0.12664	112	0.18978	152	0.24604	192	0.29539
33	0.059443	73	0.12829	113	0.19127	153	0.24736	193	0.29654
34	0.061219	74	0.12995	114	0.19276	154	0.24867	194	0.29768
35	0.062993	75	0.1316	115	0.19424	155	0.24998	195	0.29882
36	0.064764	76	0.13324	116	0.19572	156	0.25128	196	0.29996
37	0.066533	77	0.13488	117	0.19719	157	0.25258	197	0.30109
38	0.0683	78	0.13652	118	0.19866	158	0.25387	198	0.30222
39	0.070064	79	0.13816	119	0.20013	159	0.25517	199	0.30335
40	0.071826	80	0.13978	120	0.20159	160	0.25645	200	0.30447

Table 2: $\mu_1(j\pi/1000)$ vs. j, $j = 1, \ldots, 200$, by step 1.

205	0.31001	405	0.4667	605	0.54346	805	0.57978
210	0.31546	410	0.46936	610	0.54476	810	0.58031
215	0.32081	415	0.47196	615	0.54604	815	0.58084
220	0.32607	420	0.47453	620	0.54729	820	0.58135
225	0.33123	425	0.47704	625	0.54852	825	0.58185
230	0.3363	430	0.47951	630	0.54973	830	0.58233
235	0.34129	435	0.48194	635	0.55092	835	0.58281
240	0.34618	440	0.48433	640	0.55208	840	0.58328
245	0.35098	445	0.48667	645	0.55323	845	0.58372
250	0.3557	450	0.48897	650	0.55435	850	0.58415
255	0.36034	455	0.49124	655	0.55545	855	0.58458
260	0.36489	460	0.49346	660	0.55653	860	0.58499
265	0.36936	465	0.49565	665	0.55758	865	0.5854
270	0.37375	470	0.49779	670	0.55862	870	0.5858
275	0.37806	475	0.4999	675	0.55964	875	0.58619
280	0.38229	480	0.50197	680	0.56064	880	0.58636
285	0.38645	485	0.50401	685	0.56161	885	0.58669
290	0.39053	490	0.50601	690	0.56257	890	0.58701
295	0.39454	495	0.50798	695	0.56351	895	0.58733
300	0.39848	500	0.50991	700	0.56443	900	0.58763
305	0.40235	505	0.5118	705	0.56533	905	0.58793
310	0.40614	510	0.51367	710	0.56622	910	0.58821
315	0.40987	515	0.5155	715	0.56708	915	0.5885
320	0.41354	520	0.5173	720	0.56793	920	0.58877
325	0.41713	525	0.51907	725	0.56876	925	0.58904
330	0.42067	530	0.52081	730	0.56957	930	0.58931
335	0.42413	535	0.52251	735	0.57037	935	0.58956
340	0.42754	540	0.52419	740	0.57115	940	0.58956
345	0.43089	545	0.52584	745	0.57191	945	0.58978
350	0.43418	550	0.52745	750	0.57265	950	0.59
355	0.4374	555	0.52904	755	0.57338	955	0.59024
360	0.44058	560	0.5306	760	0.57409	960	0.59049
365	0.44369	565	0.53214	765	0.57479	965	0.59077
370	0.44675	570	0.53364	770	0.57547	970	0.59113
375	0.44976	575	0.53512	775	0.57614	975	0.59149
380	0.45271	580	0.53658	780	0.57679	980	0.59143
385	0.45561	585	0.538	785	0.57743	985	0.59131
390	0.45846	590	0.5394	790	0.57805	990	0.59114
395	0.46125	595	0.54078	795	0.57865	995	0.59092
400	0.464	600	0.54213	800	0.57922	1000	0.59064

Table 3: $\mu_1(j\pi/1000)$ vs. j, $j = 205, \ldots, 1000$, by step 5.